Machine Learning Approaches for Enhancing the SoH Estimation of LTO Batteries

İsmail Can Dikmen[1*] (ID), Nisanur Yıldıran[2] (ID) and Teoman Karadağ [2] (ID)

1. *TEMSA R&D Center, Adana, Türkiye*
2. *Department of Electric Electronic Engineering, Engineering Faculty, Inonu University, Malatya, Türkiye*

Abstract

Lithium titanate oxide (LTO) batteries' practical application in modern technologies depends on accurately predicting their state of health (SoH). Using advanced machine learning (ML) techniques, our study examined how to estimate LTO batteries' SoH. For this purpose, we aged rechargeable LTO batteries for 3500 cycles with a battery analyzer and performed differential voltage analysis (DVA). To estimate SoH as a regression problem, we used three machine learning methods: Artificial Neural Networks (ANN), Support Vector Machines (SVM), and Gaussian Process Regressions (GPR). As a novel approach to SoH estimation, our research uses a feedforward neural network to solve the categorization problem. In analyzing and comparing the performance of all methods, we found that this categorization-based neural network approach improved computational efficiency by 60.89% while achieving SoH estimation accuracy of 93.18%. By advancing the field of battery health monitoring, these findings contribute to more reliable and efficient battery management algorithms. In addition to improving battery management systems' accuracy and computational efficiency, the categorization approach demonstrated here could also be used to extend the life and reliability of LTO batteries, including those used in electric vehicles and renewable energy storage systems. The results of this study illustrate the importance of applying innovative machine learning applications to enhance battery SoH estimations, providing important implications for future research and practice.

Keywords: LTO batteries; Machine learning; State of Health estimation; Differential voltage analysis; Battery management algorithms

1. Introduction

Challenges such as increasing environmental pollution, increasing greenhouse gas emissions, increasing global warming, climate change, and the scarcity of available natural resources cause the use of renewable energy sources to increase daily. The electric transportation sector contributes greatly to the reduction of these problems with rapid development all over the world. Lithium-ion batteries (LIB) are the most important component in meeting the transportation needs of electric vehicles. The foundations of LIB technology were laid in the 1970s due to studies conducted by Michael Stanley Whittingham [1]. In the following years, this technology was developed and matured by a working group consisting of physicist John Bannister Goodenough, chemist Michael Stanley Whittingham, scientist Rachid Yazami, and chemist Akira Yoshino [2]. Sony commercialized LIB in 1991 [3].

LIBs have become popular in energy storage systems due to their long lifetime, lack of memory, potential to deliver dense and high energy, environmental friendliness, and relatively low maintenance. This has led to their dominance in today's energy storage market [4].

However, an effect called aging is observed in LIBs. The leading cause of battery aging is the chemical reactions between the electrolyte and the negative electrode [5,6]. Due to these chemical reactions, the conduction potential of the electrolyte decreases. This means fewer electrons and ions can be transported, and therefore, the total usable capacity of the battery decreases. This is where the concept of state of health (SoH) emerges [7,8]. SoH is the most basic parameter that informs the user about the aging characteristics of the battery. The battery's capacity to hold instantaneously is a key component for SoH detection. Determining the health status of batteries is important to increase the battery's useful life and ensure the system's safe operation [9]. Ideally, the SoH value of a factory-fresh battery is considered 100%. With calendar or cyclic aging, the battery

completes its useful life over time. To detect this, SoH determination with high accuracy is a good reference for using the system to obtain maximum efficiency [6]. Although there is no universal consensus on the definition of SoH [10], there are various definitions in the literature. SoH can be defined based on capacity [11], internal resistance [12], RUL [13], and power [14]. However, the definition based on capacity is a much more common definition. It is defined as the percentage of the ratio of the instantaneous capacity to the capacity value of the battery at the factory [15]. With the studies conducted, it has been observed that when the capacity of the battery drops below 80%, there is a serious decrease in the performance of the battery. Therefore, 80% is accepted as a reference for the end of battery life [16].

Since LIBs are nonlinear systems, the electrochemical reactions in their structure make it difficult to determine the aging characteristics of the battery. This makes SoH estimation and its high accuracy more complex. Due to the increasing use of rechargeable batteries daily, SoH estimation has attracted great interest from researchers. Various methods have been proposed for SoH estimation. When the proposed methods are examined, it is observed that various SoH categorizations are proposed [17–19]. Basically, model-based methods and data-based methods can be considered under two categories. The parameters required for applying model-based methods are obtained through data acquisition experiments performed in a laboratory environment. Parameters such as open circuit voltage (OCV), capacitance, and impedance can be obtained through these experiments. As a result of subjecting these parameters to some experimental studies, they can be sufficiently informative about the SoH of the battery. However, complex physics-based equivalent circuit model (ECM) models are needed to obtain the parameters in experimental studies. The mathematical computational burden is quite high. The model parameters are difficult to self-update and cannot quantify the uncertainty in the estimation. Although model-based methods are efficient, they are not preferred in real-time applications [20]. In data-driven methods, LIB's health monitoring is usually performed by analyzing preliminary data such as current, voltage, capacitance, and impedance. Data-driven methods have the advantages of requiring few input features for model training, being model-independent, having low relative computational cost, and using a large set of algorithms. These features have made this class of methods more preferable in recent years [20].

Recent studies have shown that the use of ML algorithms in the data-driven method category has increased rapidly. Gaussian Process Regression (GPR) [21–23], Support Vector Machine (SVM) [24,25], and Artificial Neural Network (ANN) [26,27] are some of the most widely used ML algorithms for SoH prediction in the literature.

When the literature is examined, it is seen that most of the studies on SoH are carried out with lithium-iron-phosphate (LFP), nickel-cobalt-aluminum (NCA), and nickel cobalt manganese (NMC) batteries. Niraula et al. [28] achieved high accuracy in SoH estimation with an error rate of 2.5% using NMC

battery chemistry. This study emphasizes the effectiveness of data-driven techniques for portable applications. In Tang et al.'s study [29], an algorithm developed in experiments on four different battery chemistries (LFP, NMC, LCO, NCA) achieved high accuracy in SoH estimation with an error rate of 1.2%. This method calculates SoH values by analyzing regional capacity and voltage variations. In Li et al.'s study [30], Panasonic NCR 18650B LIB are investigated using electrochemical impedance spectroscopy (EIS) at various states of charge, and SoH estimation is performed with an ANN model with high accuracy with an error rate of 1.2%. Huang et al. [31] used the local frequency method to estimate LIB' SOH. This method is applied to NCA and LFP battery chemistries and achieves high accuracy at low sampling frequencies. SOH models based on regional voltage values achieved R-squared values of more than 0.99%, proving the method's effectiveness. In Müller et al. In a study [32], the effects of mechanical pressure on the performance and aging of LIB's are investigated. Experiments on 1.4 Ah graphite/NMC622 LIB's showed how mechanical pressure at the electrode and cell level can improve and slow down electrochemical performance and aging processes.

However, it has been observed that there are not enough academic studies on SoH analysis of lithium titanate oxide (LTO) battery chemistry.

Mahdi Soltani [33] et al. used a nonlinear Feed Forward Neural Network (FFNN) and presented an accurate SoH prediction and end-of-life (EoL) prediction model for LTO cells. They demonstrated that the SoH of LTO battery can be predicted with 5% accuracy or <250 FEC (Full Equivalent Cycle) prediction error. Chaoui and Ibe-Ekeocha [34] developed a battery analysis model for LFP and LTO batteries using dynamically directed recurrent networks (DDRNs). The model is based on Nonlinear Autoregressive with Exogenous Inputs (NARX) architecture and estimates the State of Charge (SoC) and SoH of the battery using parameters such as battery voltage, charge/discharge currents, and environmental temperature.

To contribute to the literature at this point, the software we developed in Python is used to pre-process the aging data of LTO batteries. With the processed data, differential voltage analysis (DVA) in MATLAB environment is handled with a new approach. In the paper that used this method in the literature, DVA is used together with a regression method to calculate SoH. Especially for LFP batteries, the cycle value and capacity value have a linear pattern within a certain range so that the calculations can be done quickly [35]. However, from the results obtained in this study, it is determined that the cycling and capacity loss do not have a linear correlation. Therefore, a new approach has been developed based on the cycle value for SoH calculation for LTO batteries. Subsequently, the problem setup is discussed under two main headings. As the first main topic, SoH estimation is considered a regression problem. Linear Support Vector Machine (LSVM), Rational Quadratic Gaussian Process Regression (RQGPR), and ANN methods are used to solve this regression problem. As the second main issue, the problem is

treated as a categorization problem. The feed-forward neural network method is used to solve the SoH calculation problem. This is the first time in the literature that this problem is treated as a categorization problem. The performance analysis of all these algorithms for determining the SoH of LTO batteries is carried out separately, and the results are presented comparatively.

The rest of the paper is organized: Section 2 provides experimental descriptions, the SoH definition, and methodology details. Section 3 presents the results and discussions. Section 4 presents the proposed methodology. Section 5 summarizes the conclusions.

2. Material and Method

2.1. Experiment setup

Huahui New Energy HTC Series 18650 LTO batteries are used in this study. The batteries used for this test are rechargeable LTO 18650 cells with specifications and aging conditions specified in Table 1. The test data used are obtained through the battery test setup, which includes the NEWERA BTS4000 Battery Analyzer tester, a computer for user-machine interface and data storage, and the battery cells. Seven LTO battery cells with the same charge and discharge rate are used for comparison and validation. The cells are charged and discharged at constant rates in each aging cycle under specified conditions. The batteries are gradually aged for 3500 cycles. The data sets obtained from the static capacity test with a 0.8 C rate are mainly used in this study.

Table 1. Material properties of SCP10.

Battery Chemistry	Battery Geometry	Nominal Capacity (mAh)	Nominal Voltage (V)	C Rate	Cycle Numbers	Battery Label
Lithium Titanate Oxide (LTO)	Cylindrical (supercapacitor) 18650	1200	2.5	0.8	500	Cell 1
					1000	Cell 2
					1500	Cell 3
					2000	Cell 4
					2500	Cell 5
					3000	Cell 6
					3500	Cell 7

2.1.1 Lithium titanate oxide battery (LTO)

LTO battery chemistry is a battery chemistry in the category of lithium-based rechargeable batteries with a widely used application. LTO batteries have also found wide commercial use in wristwatches, electric vehicles, and bicycles [36].

The chemical formula of the LTO battery is $Li_4Ti_5O_{12}$. The reaction showing the chemical production of the formula is bi-directional and is presented in Eq. (1). The chemical reaction can be expressed as breaking of $Li_7Ti_5O_{12}$ into 3 units of Li^+ and the release of $3e^-$.

$$Li_7Ti_5O_{12} \leftrightarrow Li_4Ti_5O_{12} + 3Li^+ + 3e^- \qquad (1)$$
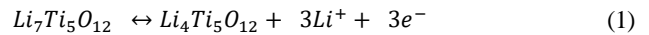
LTO batteries are increasingly used because they have a high cycle range, are safe, and have features such as fast charging due to the high charge/discharge rate. The batteries used in this study are Huahui New Energy HTC Series LTO batteries, which are in the 18650 cylindrical battery category according to the IEC/EN60086 standard. These batteries' rated capacities are typically 1300 mAh and a minimum of 1200 mAh. According to the battery analyzer data, it is measured as 1207.3 mAh (0.8C). The internal impedance of these batteries is less than 35 mΩ. Rated voltages are minimum discharge voltage 1.5V, nominal voltage 2.4V, and maximum charge voltage 2.8V. The maximum discharge current is 10C, that is, 13A. As the casing is 18650, the height of the battery is 65.5 mm, and the diameter is 18.5 mm. Its weight is 38.5±1 g. The image of the battery is presented in Figure 1.

Figure 1. Huahui New Energy HTC Series LTO Battery

2.1.2. Battery analyzer

The data used in the study are obtained by aging the batteries with the BTS4000-5V6A battery analyzer, as shown in Figure 2. The instrument has 0.05% full-scale accuracy. Current output ranges are 5mA-1A, 1A-6A, and 6A-12A. The constant voltage-breaking current ranges are 2mA, 12 mA, and 24 mA. The constant voltage output range is between 25mV and 5V. It has a data recording frequency of up to 10 Hz, and its signal-to-noise ratio is less than 85dB. The device is designed for the prismatic, pouch, and cylindrical batteries. Due to the characteristics of the batteries used in the study, the minimum discharge voltage is determined as 2V, and the maximum charge voltage is determined as 2.8V.

Figure 2. BTS4000-5V12A battery tester

2.2. State of health

Batteries' performance decreases over time depending on their cyclic aging frequency, storage conditions, and calendar aging periods. In batteries with declining health, a decrease in

capacity and, consequently, an increase in internal resistance is inevitable.

SoH is one of the most critical parameters in LIB's battery condition category. It is generally defined depending on internal resistance and capacity. Since it is often defined as capacity-dependent, it can be expressed as given in Eq. (2).

$$SoH = \frac{C_{current}}{C_{nominal}} x \ 100\% \tag{2}$$

Here, $C_{current}$ represents the instantaneously measured capacity value, and $C_{nominal}$ represents the capacity value that matches the battery's factory conditions. SoH varies depending on the electrochemical reactions occurring in the battery structure. However, it also varies depending on parameters such as temperature, storage conditions, and pressure, which are considered external factors [37]. When the capacity value drops below 80%, it is accepted as an indicator that the battery is no longer suitable for use [38].

2.3 Differential voltage analysis (DVA)

DVA is a method developed for the electrical identification of battery cells. Numerous studies in the literature use DVA to calculate SoH [39–41]. It is expressed by taking the derivative of the voltage concerning the capacitance and writing it as a function of the voltage [42]. The potential difference of the battery cell can be defined as the difference between the anode and cathode potentials, as in Eq. (3).

$$V_{cell} = V_{cathode} - V_{anode} \tag{3}$$

A derivative expression of the cell's capacity against voltage can be defined as a $\left(\frac{\partial C}{\partial V}\right)_{cell}$, and Eq. (4) can be obtained by considering Eq. (4). In this way, the capacity decrease can be observed graphically.

$$\left(\frac{\partial C}{\partial V}\right)_{cell} = \left(\frac{\partial C}{\partial V}\right)_{cathode} - \left(\frac{\partial C}{\partial V}\right)_{anode} \tag{4}$$

2.4. Artificial neural network (ANN)

ANN is a method designed and inspired by the functioning of the nervous system of human physiology, namely neurons, and developed for machines to learn with a similar logic. The pioneers of the ANN approach are Walter Pitts and Warren McCulloch. The foundations of ANN were laid in 1943, and these researchers studied it [43]. Perceptron, the most basic and primitive form of ANN, which can be considered the first functional ANN, was presented by Rosenblatt in 1957. ANNs can be compared to a sandwich because they consist of n hidden layers between input and output layers. In ANN, inputs are generally expressed as "x" and outputs as "Y". The x's first enter the input layer. They are then subjected to some processing and exit the layer as layer output "y". ANNs are widely used in different fields to predict a battery's health state, parallel with technological advances [44,45].

ANN will classify cases where the output variable is an ordered binary. If the output variables are not continuous but limited, this can be considered a classification problem. The purpose of classification ANNs can be defined as categorizing the analysis made on the data as a function of the input parameters belonging to a particular class. Regression ANNs, on the other hand, predict an output variable as a function of the inputs. In regression ANNs, the mathematical calculations of neurons can be expressed as given in Eq. (5). Among the parameters used in Eq. (5), w weight, x inputs, b bias coefficient, y_1 refers to the output of neuron number 1 in the hidden layer.

$$y_1 = f_{act}(w_1 x_1 + w_2 x_2 + w_3 x_3 + \cdots + w_{302} x_{302} + b) \tag{5}$$

$$Y = f_{act}\left(\sum_{i=1}^{295} (w_i \times y_i) + b\right) \tag{6}$$

Among the parameters used in Eq. (6), w represents weight, b bias coefficient, Y output function, and f_{act} activation function. The x inputs are multiplied by a weight and sent to the neurons in the hidden layer. The neuron in the hidden layer takes the sum of all the inputs multiplied by the weights, adds a bias, and then puts it into the activation function to produce the output y. When the neural network is used for regression, there is only one output neuron. This neuron sums the outputs from neurons in the hidden layer multiplied by the relevant weight and adds bias. The regression output Y of the ANN is calculated by putting the result into the activation function.

In this study, the Rectified Linear Unit (ReLU) function presented in Eq. (7) is used as the activation function.

$$f_{act}(x) = \begin{cases} 0, & x < 0 \\ x, & x \geq 0 \end{cases} \tag{7}$$

Another activation function used in this study is the Softmax function, which is presented in Eq. (8).

$$\sigma(x)_i \frac{e^{x_i}}{\sum_{j=1}^{T} e^{x_j}} \ for \ i = 1, \dots, T \ and \ x = x_i, \dots, x_T \in \ R^T \tag{8}$$

2.5. Support vector machines (SVM)

SVM is an algorithm used in ML to solve regression and categorization-based problems. Vladimir N. Vapnik and Alexey Chervonenkis first developed it in [46,47]. Burger also presented a comprehensive study on using SVs for classification in 1998 [48].

SVM is widely used in the literature to solve technical problems, such as analyzing battery health status and estimating their remaining useful life [49].

The implementation of SVM in solving categorization problems is based on the principle that the data corresponds to points

in an n-dimensional space, which are categorized within themselves with the hyperplane. SVM is also widely used in solving regression problems.

2.6 Support vector regression (SVR)

SVR is a variant of SVM used mainly for classification purposes and analysis of nonlinear situations. They can make inferences and train by generalizing. Finding the $f(x)$ function with a maximum deviation of ε from the actual target provided by the data obtained through all the training data can be defined as the main objective of the SVR. The function should be as flat as possible. In other words, the error does not matter if the error is less than epsilon ε.

The literature includes studies using SVR for various technical problems [50]. These technical problems include predicting the health state of batteries [51,52].

$S = \{(x_1, y_1), \cdots, (x_i, y_i)\}, x_i \in R^n, y_i \in R$ sample set is defined. In this defined set, x_i is the eigenvector of the ith sample, y_i is the regression value of the ith sample. N can be defined as the number of samples and n as the size of the input vector. Thus, the SVR function can be expressed as in Eq. (9).

$$f(x) = w\Phi(x) + b \qquad (9)$$

As the output $f(x)$ in Eq. (9), w can be defined as the weight vector $\Phi(x)$ as the mapping function moved to the upper dimension and b as the deviation value. At this point, it is possible to determine w and b parameters using the objective function.

$$minR(F) = \frac{1}{2}\|w\|^2 + C\sum_{i=1}^{n}|f(x_i) - y_i|_\varepsilon \qquad (10)$$

Here, C is the penalty factor, n is the number of training samples, $f(x_i)$ i^{th} is the predicted value corresponding to the sample. y_i i^{th} is the actual value of the sample, ε is the maximum acceptable regression error, that is, the threshold value.

$$|f(x) - y|_\varepsilon = maks\{0, |f(x) - y| - \varepsilon\} \qquad (11)$$

The definition of the optimization problem of the target function can be written as follows Eq. (12);

$$min\frac{1}{2}\|w\|^2 + C\sum_{i=1}^{N}(\xi_i + \xi*_i), \quad i = 1,2,\dots,N \qquad (12)$$

In cases where ξ_i and ξ_1^* i^{th} training samples have relaxation variables; C is the penalty factor. Relaxation is a modeling strategy in mathematical optimizations. It can be defined as bringing the difficult problem closer to the easy one. The solution with these parameters provides information about the main problem. ξ_i and ξ_1^*, ε and $f(x_i)$ the constraints between them can be expressed in Eq. (13) as:

$$s.t = \begin{cases} y_i - f(x_i) \leq \varepsilon + \xi_i \\ f(x_i) - y_i \leq \varepsilon + \xi*_i \\ \xi_i, \xi*_i \geq 0 \end{cases} \qquad (13)$$

The regression functions parameters α_i and α_i^* the LaGrange multipliers, x_i, and x_j are training sample and input sample vectors.

$$f(x) = \sum_{i=1}^{N}(\alpha_i - \alpha*_i)K(x_i, x_j) + b \qquad (14)$$

Here, $K(x_i, x_j)$ is the kernel function. Gaussian kernel function is presented in Eq. (15).

$$K(x_i, x_j) = e^{\frac{(-\|x_i - x_j\|^2)}{2\sigma^2}}, \qquad \sigma > 0 \qquad (15)$$

When using SVR as a model, the C penalty factor regulates the generalization potential of the model. σ is used as a kernel function width parameter to control adaptability. If these parameters are selected appropriately, estimation performance can be noticeably improved. As a result, the appropriate selection of parameters can prevent possible erroneous estimations [51].

2.7. Gaussian process regression (RQGPR)

When the estimation approach with Gaussian processes is examined, it is noticed that it is not a new topic. Its origins date back to the 1940s [53]. GPR, which has a probabilistic approach, has recently started to attract attention with its applications in both statistical and engineering problems compared to nonlinear modeling approaches [54,55]. Although GPR is generally used to explain static nonlinearity, it also finds application in dynamic processes for modeling purposes [56]. Williams and Rasmussen first used GPR in ML in 1996.

GPR is a highly effective ML method for solving the complex and challenging problem of predicting the aging characteristics of batteries. It has a non-parametric structure. Thus, it has a flexible structure in detecting non-linear system relationships. Its flexible structure can directly determine the estimation uncertainties. Various combinations of GPR are suitable for predicting the behavior of a system under specified conditions. It is also widely used in SoH prediction studies [57–59]. Gaussian processes have a Gaussian distribution with finite sets of variables. This is an essential factor in making highly accurate predictions [60]. The covariance function and the mean function define the Gaussian process. For a process $f(x)$, the mean function is defined as $m(x)$, and the covariance function is defined as $k(x, x')$. The definition of the Gaussian process is given in the Eq. (16);

$$f(x) \sim GP(m(x), k(x, x')) \qquad (16)$$

The mean and covariance functions written in the equation are given in Eq. (17);

$$m(x) = E[f(x)]$$

$$k(x, x') = E[(f(x) - m(x))(f(x') - m(x'))] \qquad (17)$$

One of the powerful features of the GPR model is that it can work with all kinds of covariance functions. The covariance of the GPR is defined in terms of a kernel. There are different types of kernels, such as linear, periodic, and rational quadratic. However, the most preferred kernels in practice are Squared Exponential (SE), Matérn, and Rational Quadratic (RQ). The kernels used provide advantages depending on the data and the characteristics of the problem. This study uses Rational Quadratic GPR, which accurately predicts SoH.

The Rational Quadratic kernel is a kernel function suitable for data with multi-scale features and flexible in modelling variations with non-identical length scales. The mathematical expression of the RQ kernel can be defined as given in Eq (18);

$$k(x_i, x_j) = \sigma_f^2 (1 + \frac{(\|x_i - x_j\|)^2}{2\alpha \ell^2} \qquad (18)$$

In the given equation, σ^2 is the kernel variance. l defines the length scale. α is the scale mixing parameter. These three parameters play an active role in determining how the RQ kernel captures different features in the data and the model's flexibility. Here $K(x_i, x_j)$ is the kernel function. The rational Quadratic kernel function is presented in Eq. (17). σ_f corresponds to σ_f in the same way, α and ℓ.

3. Results & Discussions

In the study, seven LTO battery cells are aged 500-3500 cycles range in the battery analyzer. In the battery analyzer, the minimum discharge voltage is set to 1.3V, the maximum charge voltage is set to 2.75V, and the aging process is carried out at 0.8 C. In addition, 10-minute rests are added between the charging and discharging processes. It took approximately 5.5 months to complete all these processes and to obtain the data used for training ANNs in the study. The capacity fades depending on the cycle, as presented in Figure 3.
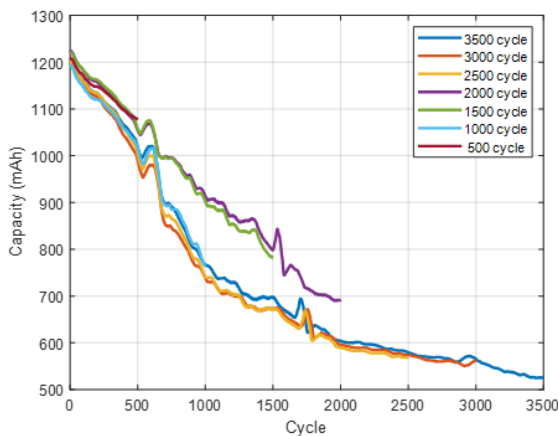

Figure 3. Capacity fade of various cycles

Preprocessing is done using tailored software prepared in Python to make the obtained data suitable for our study. Voltage values and capacity values for each cycle are combined within themselves. Then, these processed voltage and capacity data are transferred into MATLAB. Subsequently, DVA is performed in MATLAB. While performing the analysis, a filtering process is applied to remove the noise in the data. The calculated $\partial C/\partial V$ and $\partial V/\partial C$ data are filtered with a frame size 30 sliding window moving average filter.
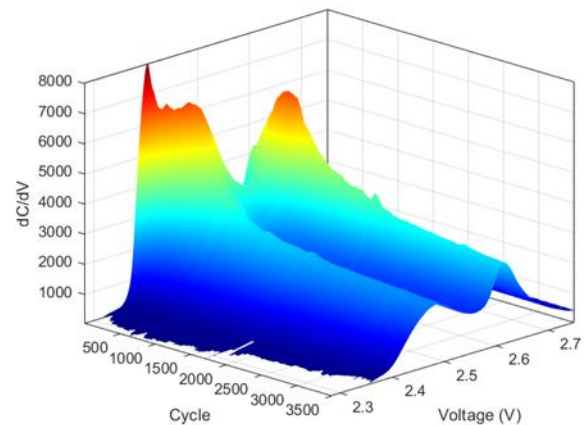

Figure 4. dC/dV data according to voltage data and cycles

Afterward, the graphs of the obtained data are drawn against capacity and voltage. Graphs of calculated $\partial C/\partial V$ data are presented in Figure 4 according to voltage and Figure 5 according to capacity.

In Figure 4, voltage is presented on the x-axis, cycle on the y-axis, and $\partial C/\partial V$ on the z-axis. Here, the energy-holding capacity corresponding to the same voltage value decreases as the cycle increases.

However, as seen in the graph, the decrease in capacity corresponding to the voltage does not have a linear correlation with the cycle. Figure 4 It is seen from Figure 4 that the battery stability is very high up to 1000 cycles, and then it goes to worse values. When the $\partial C/\partial V$ graph of LTO is considered, it is seen that two different cathodic peaks are related to different Li environments in the lattice structure. The redox peak voltage values with increasing cycling up to 3500 cycles are decreased, which means the lattice structure deformation during the lithation and delithation process.

Figure 5 shows the graph where $\partial C/\partial V$ is plotted according to voltage. Here, the graph is drawn separately for 1, 500, 1000, 1500, 2000, 2500, 3000, 3500 cycles of a single cell. When the curves are examined, it is seen that there are two peaks in all curves. It is seen that both peaks in all curves, except the first cycle, correspond to a specific voltage value. These voltage values are calculated as 2.475V for the first peak and 2.625V for the second peak. We predicted that the increasing voltage value by cycling is related to the change in the local environment of the Li-ions in the lattice. The low-voltage Li-site in the lattice has more deformation than the high-voltage Li-site in the lattice.
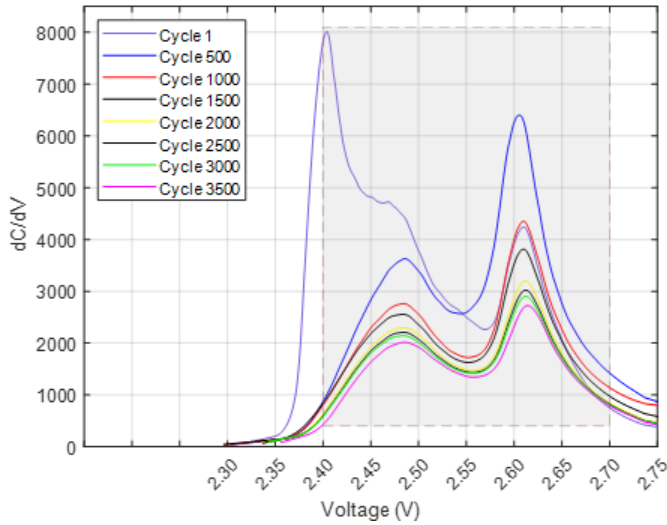
Figure 5. dC/dV – Voltage graph.

In these studies, the data obtained from the DVA analysis are plotted according to the capacity. The results obtained when the same analysis is performed for LTO batteries are presented in Figure 6 and Figure 7. When the data of $\partial C/\partial V$ are plotted according to capacity, two peaks are detected in the graphs. The distance between these two peaks gives the battery's remaining capacity, namely the SoH, since the graph is drawn according to the capacity. As the batteries age, one of the peaks remains stable, while the other one shifts to the left according to the aging rate, in other words, according to the number of cycles. This shows the aging effect on the battery. However, this method has been used successfully only for LFP batteries in the literature.
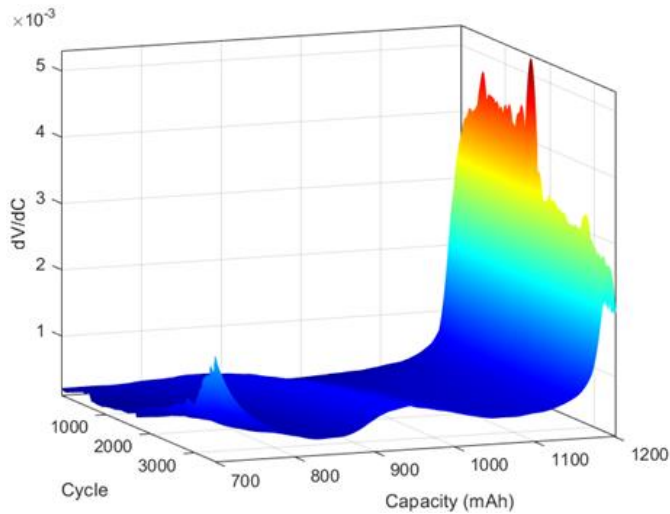

Figure 6. dV/dC – Capacity 3D view

Since it is impossible to calculate the 0%-100% SoH value in the study, as mentioned earlier, the 80%-100% SoH range, which is the practical use value, is taken as a basis. In this study, the same method is applied to LTO batteries. However, no shift is observed at the peak even if the capacity is taken in the range

of 0.8-1. This can be clearly seen in Figure 7 and Figure 8. Therefore, it is concluded that the earlier method does not apply to the LTO batteries used in this study.
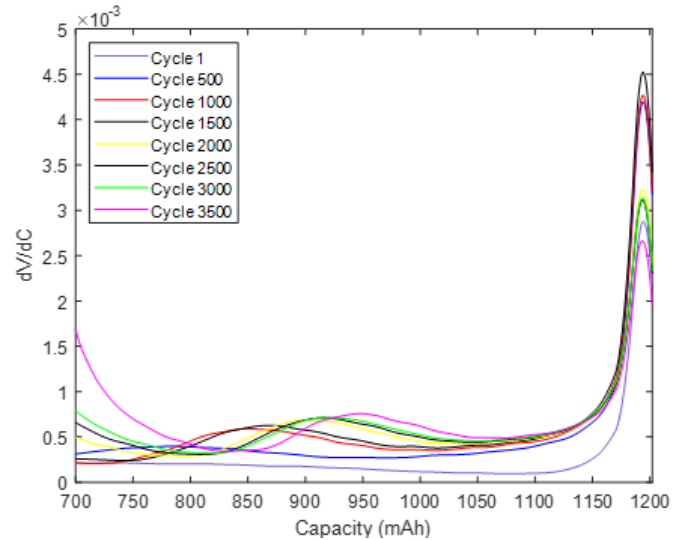

Figure 7. dV/dC – Capacity graph.

When the methods used for health state analysis of batteries are examined in the literature, it is seen that the DVA method is used together with ANN, SVM, and GPR methods, which are among the ML methods. These methods are analyzed separately based on applicability for LTO batteries. The analysis aims to determine the cycle count of the battery, which is directly related to the SoH. For this reason, in the study, the cycle count corresponding to the health state is calculated as output.

First, the aging data obtained from LTO batteries are processed to determine the voltage values corresponding to the peaks of the two ridges observed in the $\partial C/\partial V$ graphs. Accordingly, the voltage of the first peak is determined as 2.475V, and the voltage of the second peak is determined as 2.625V. The data is divided into voltage ranges 2.4V-2.55V and 2.55V-2.7V To include both peaks. The training data set is prepared by combining the two data sets obtained. Data from two battery cells, 3500 and 2500 cycles, are used in the training dataset. The data of the other five batteries are used for validation. The training data set is subjected to regression analysis with SVM, GPR, and ANN algorithms in MATLAB Regression Learner.

MSE is a measure of error determined by averaging the square of the difference between the actual and predicted values. It is primarily used in regression analysis problems when estimating with continuous variables. It is also used to form a common ground for comparing the different algorithms. It is used to determine the quantitative success of the model. It is calculated using the formula given in Eq. (19).

$$k(x_i, x_j) = \sigma_f^2 (1 + \frac{(\|x_i - x_j\|)^2}{2\alpha\ell^2} \qquad (19)$$

In this equation, n is the number of data points, Y_i is the actual value, $\hat{Y}_i$ is the predicted value. RMSE is the square root of MSE.

$$RMSE = \sqrt{\frac{1}{n}\sum_{i=1}^{n}(Y_i - \hat{Y}_i)^2} \qquad (20)$$

3.1. SVM regression implementation

The training dataset is subjected to the SVM algorithm. The computational cost of the linear SVM algorithm is found to be lower than other kernel functions. However, even in the optimal case, the lowest error rate calculated is 20 MSE. When the SVM kernel function is chosen as Gaussian, and the data is standardized while its parameters are set as kernel scale 6.9352, box constraint 975.9178, epsilon 0.44775, the regression could be made with an error rate of 1.2353 MSE. As a result of the analysis, it has been observed that obtaining a better result than 1.2353 MSE with the SVM algorithm is impossible.

3.2 GPR implementation

GPR kernel function Rational Quadratic is chosen, the training data set is standardized, and kernel function parameters are set as ℓ =20.1264327950019, α =1.05431948363457, σ_f = 588.287390875263. Thus, it has been observed that the RQGPR algorithm can regress with an error rate of 0.77322 MSE. However, according to the analyses, obtaining a better result than 0.77322 MSE with the RQGPR algorithm is impossible.

3.3 ANN implementation

The trilayered ANN algorithm is trained using a training dataset. When the ANN activation function is selected, ReLU, and the data are standardized, and the ANN is designed to have 10 neurons in each of the three layers, it can regress with an error rate of 48,384 MSE. However, according to the analyses made, it is not possible to obtain a better result than 48,384 MSE using the ANN algorithm using this data set.

4. Proposed Method

In the literature, there are studies on the onboard applicability of ML methods, especially ANN, for battery management system functions [61–63]. In this study, the comparison between RQGPR, LSVM, and ANN regression algorithms is based on the test conducted on a laptop computer with an Intel Core i7-7700HQ 2.80 GHz processor and 16 GB of RAM. All algorithms run 1500 times to do that, and the average execution time is calculated. According to the results obtained, the execution times of the algorithms are as RQGPR 0.0179 sec, LSVM 0.0119 sec, and ANN 0.0122 sec.

ANNs can also be used to solve pattern recognition problems with a categorization problem approach rather than regression. When the problem addressed in this study is considered a pattern recognition problem, the data presented in Figure 4 obtained from DVA can solve a cascading categorization problem. In other words, if the 1000-cycle data is divided into 20% slices, SoH can be calculated within ±200 cycles. When this 20% slice is divided into 20% slices, the sensitivity drops to ±40 cycle.

The ANN is trained with the first 1000 cycles of aging data containing 0.8-1.0 SoH values of 6 LTO batteries. In this way, the DVA data of a given cycle can be used to calculate which of the cycle classes (1-200, 201-400, 401-600, 601-800, and 801-1000) the sample belongs to.

This process uses a two-layer feed-forward neural network with 302 input neurons, five output neurons, and a varying number of hidden neurons for each specified range. In the optimized ANN design, sigmoid functions for hidden neurons and softmax functions for output neurons are chosen as activation functions.

While determining the hidden layer size, the number of neurons is selected in the range of 0-300 to keep the operational cost low. The error rate is calculated by training the ANN separately for each neuron count. In Figure 8, the graph showing the error rate according to the hidden layer size is presented. The number of neurons that gave the lowest error rate is determined to be used in the study. As a result, the hidden layer size for the first level ANN is set to 72 for the minimal error value as presented in the graph.
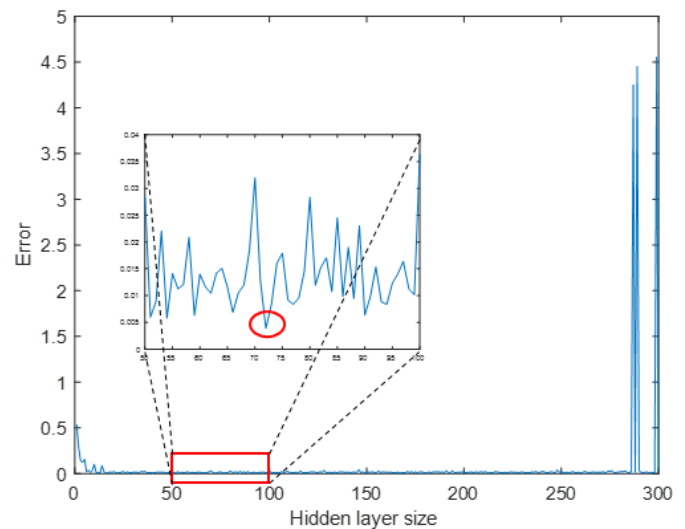
Figure 8. Optimal hidden layer neuron number for 1st level ANN

Figure 9 presents the results obtained from the ANN trained with 72 hidden neurons. There are 6000 observations here. Each observation collects data by charging/discharging the battery from 0% SoC to 100% SoC. 70% of this data is used for training, 15% for validation, and 15% for testing. According to the results, the Level 1 cycle class can be determined with 99.7% accuracy.

After determining which quintile is in the SoH category at the first level, the second-level cycle class (1-40, 41-80, 81-120, 121-160, 161-200) can be calculated. A similar design to the first-level ANN is used for this process. That is a two-layer feed-forward network with 302 input neurons, five output neurons,

and 39 hidden neurons. According to the results obtained, the cycle category of the first 20% can be determined with 99% accuracy. As a result, the cycle of the battery's aging can be specified with a margin of error of 1.3% with the 2-layer cascade ANN.

Figure 9. Results of the 1st level ANN with optimal hidden layer size:72

5. Conclusions

In this study, regression algorithms (SVM, GPR, and ANN) based on DVA are applied separately to solve the SoH problem for LTO batteries, and the results are presented comparatively. For this purpose, 7 Huahui LTO batteries are aged at different rates, with a maximum of 3500 cycles in the analyzer. DVA is performed with the obtained data. The data of 2500-cycle and 3500-cycle batteries are used to train artificial intelligence algorithms. The data of the remaining batteries are used for testing and validation purposes.

DVA is a method that has been used successfully in calculating SoH for batteries with LFP chemistry. This method is preferred in terms of ease of application. Because it is based on the voltage and capacity values measured by BMS, it has been concluded that the algorithms successfully applied for LFP batteries in the literature cannot be applied in the same way for LTO batteries. This is because of the different behavior patterns of the peaks observed as a result of DVA due to the unique characteristics of the battery chemistries' electrochemicals. For example, in LFP batteries, as the cycle increases, that is, as the battery ages, the voltage value corresponding to the maximum energy retention changes. However, as LTO batteries age, the voltage

value corresponding to the maximum energy retention remains constant.

SVM, GPR, and ANN algorithms for calculating SoH for LTO batteries with DVA analysis are discussed in this study. According to the results, the highest accuracy rate is achieved with the RQGPR algorithm. However, it has been observed that the computational cost of the RQGPR algorithm is relatively high compared to other algorithms. With the proposed method, ANNs can be determined in 0.007 seconds with 93.18% accuracy by using a cascade. As a result of the analyses, it has been determined that the operational cost of LSVM, one of these regression methods, is 33.52% lower than the other. However, the proposed method has been observed to have a lower operational cost of 60.89%. If the SoH calculation problems of LTO batteries are to be solved with a categorization-based approach, the proposed method is considered to give optimal results; if it is desired to be solved with a regression approach, the LSVM method is considered to give optimal results.

Acknowledgment

Nomenclature

$C_{current}$	: Current capacity
$C_{nominal}$	: Nominal capacity
V_{cell}	: Cell voltage
V_{anode}	: Anode voltage
$V_{cathode}$	: Cathode voltage
y_n	: Output of neuron number n in the hidden layer
w	: Weight
x	: Inputs in ANN
b	: Bias coefficient in ANN
f_{act}	: Activation function
Y	: Outputs in ANN
y_i	: Output of neuron number i^{th} in the hidden layer
$\sigma(x)_i$	: Softmax function
$f(x)$	: Output of SVR
$\Phi(x)$	: Mapping function
C	: Penalty factor
n	: Number of training samples
$f(x_i)$	: i^{th} predicted value corresponding to the sample
y_i	: i^{th} is the actual value of the sample
ε	: Maximum acceptable regression error
ξ_i and ξ_I^*	: i^{th} training samples have relaxation variables
b	: Deviation value
α_i and α_i^*	: Lagrange multipliers
x_i	: Training samples vector
x_j	: Input samples vector
$K(xi, xj)$	: Kernel function
σ	: Kernel width
$m(x)$	: Mean function

$k(x, x')$: Covariance function
$E[]$: Expectation function
σ^2 : Kernel variance
l : Length scale
α : Scale mixing parameter

Conflict of Interest Statement

The authors declare that there is no conflict of interest in the study.

CRediT Author Statement

İsmail Can DİKMEN: Conceptualization, Writing, Analysis.
Nisanur YILDIRAN: Writing the original draft, data curation, and validation.
Teoman KARADAĞ: Supervision, validation, intellectual content.

References

[1] Whittingham MS. Electrical Energy Storage and Intercalation Chemistry. Science . 1976 Jun;192(4244):1126–7. https://doi.org/10.1126/SCIENCE.192.4244.1126.

[2] Mizushima K, Jones PC, Wiseman PJ, Goodenough JB. LixCoO2 (0<x<-1): A new cathode material for batteries of high energy density. Mater Res Bull. 1980 Jun 1;15(6):783–9. https://doi.org/10.1016/0025-5408(80)90012-4.

[3] Che Y, Deng Z, Lin X, Hu L, Hu X. Predictive Battery Health Management with Transfer Learning and Online Model Correction. IEEE Trans Veh Technol. 2021; 1;70(2):1269–77. https://doi.org/10.1109/TVT.2021.3055811.

[4] Hosen MS, Jaguemont J, Van Mierlo J, Berecibar M. Battery lifetime prediction and performance assessment of different modeling approaches. iScience. 2021;19;24(2). https://doi.org/10.1016/J.ISCI.2021.102060.

[5] Buğday N, Altın S, Karadağ T, Yaşar S. The production and electrochemical properties of N-doped porous carbon structure-based supercapacitor coin cells and flexible wristbands. J Energy Storage. 2022;1;48:103698. https://doi.org/10.1016/J.EST.2021.103698.

[6] Nelson JP, Bolin WD. Basics and Advances in Battery Systems. IEEE Trans Ind Appl. 1995;31(2):419–28. https://doi.org/10.1109/28.370294.

[7] Feder DO, Croda TG, Champlin KS, McShane SJ, Hlavac MJ. Conductance testing compared to traditional methods of evaluating the capacity of valve-regulated lead/acid batteries and predicting state-of-health. J Power Sources. 1992 Dec;40(1–2):235–50. https://doi.org/10.1016/0378-7753(92)80056-H.

[8] Huet F. A review of impedance measurements for determination of the state-of-charge or state-of-health of secondary batteries. J Power Sources. 1998;70(1):59–69. https://doi.org/10.1016/S0378-7753(97)02665-7.

[9] Bavand A, Khajehoddin SA, Ardakani M, Tabesh A. Online Estimations of Li-Ion Battery SOC and SOH Applicable to Partial-Charge/Discharge. IEEE Trans Transp Electrif. 2022;8(3):3673–85. https://doi.org/10.1109/TTE.2022.3162164.

[10] Tian J, Xu R, Wang Y, Chen Z. Capacity attenuation mechanism modeling and health assessment oflithium-ion batteries. ENERGY. 2021 Apr;221. https://doi.org/10.1016/j.energy.2020.119682.

[11] Le D, Tang X. Lithium-ion Battery State of Health Estimation Using Ah-V Characterization. Annu Conf PHM Soc. 2011;3(1). https://doi.org/10.36001/PHMCONF.2011.V3I1.2073.

[12] Dai H, Wei X, Sun Z. A new SOH prediction concept for the power lithium-ion battery used on HEVs. 5th IEEE Veh Power Propuls Conf VPPC '09. 2009;1649–53. https://doi.org/10.1109/VPPC.2009.5289654.

[13] Barré A, Deguilhem B, Grolleau S, Gérard M, Suard F, Riu D. A review on lithium-ion battery ageing mechanisms and estimations for automotive applications. J Power Sources. 2013 Nov 1;241:680–9. https://doi.org/10.1016/J.JPOWSOUR.2013.05.040.

[14] Shahriari M, Farrokhi M. Online state-of-health estimation of VRLA batteries using state of charge. IEEE Trans Ind Electron. 2013;60(1):191–202. https://doi.org/10.1109/TIE.2012.2186771.

[15] Pan S, Fulton LM, Roy A, Jung J, Choi Y, Gao HO. Shared use of electric autonomous vehicles: Air quality and health impacts of future mobility in the United States. Renew Sustain Energy Rev. 2021; 1;149:111380. https://doi.org/10.1016/j.rser.2021.111380.

[16] Yao L, Xu S, Tang A, Zhou F, Hou J, Xiao Y, et al. A Review of Lithium-Ion Battery State of Health Estimation and Prediction Methods. World Electr Veh J. 2021; 10;12(3):113. https://doi.org/10.3390/WEVJ12030113.

[17] Ge MF, Liu Y, Jiang X, Liu J. A review on state of health estimations and remaining useful lifeprognostics of lithium-ion batteries. MEASUREMENT. 2021 Apr;174. https://doi.org/10.1016/j.measurement.2021.109057.

[18] Zou Y, Lin Z, Li D, Liu Z. Advancements in Artificial Neural Networks for health management ofenergy storage lithium-ion batteries: A comprehensive review. J ENERGY STORAGE. 2023 Dec;73(C). https://doi.org/10.1016/j.est.2023.109069.

[19] Sui X, He S, Vilsen SB, Meng J, Teodorescu R, Stroe DI. A review of non-probabilistic machine learning-based state of healthestimation techniques for Lithium-ion battery. Appl Energy. 2021;300. https://doi.org/10.1016/j.apenergy.2021.117346.

[20] Basia A, Simeu-Abazi Z, Gascard E, Zwolinski P. Review on State of Health estimation methodologies for lithium-ionbatteries in the context of circular economy. CIRP J Manuf Sci Technol. 2021;32:517–28. https://doi.org/10.1016/j.cirpj.2021.02.004.

[21] Feng H, Shi G. SOH and RUL prediction of Li-ion batteries based on improved Gaussianprocess regression. J POWER Electron. 2021;21(12):1845–54. https://doi.org/10.1007/s43236-021-00318-5.

[22] Yang D, Zhang X, Pan R, Wang Y, Chen Z. A novel Gaussian process regression model for state-of-health estimation of lithium-ion battery using charging curve. J Power Sources. 2018;384:387–95. https://doi.org/10.1016/J.JPOWSOUR.2018.03.015.

[23] Yildiran N, Dikmen IC, Karadag T. State of Health Estimation of Lithium Titanate Oxide Batteries Through Data-Driven Techniques and Machine Learning. 8th Int Artif Intell Data Process Symp IDAP. 2024. https://doi.org/10.1109/IDAP64064.2024.10711165.

[24] Yang B, Qian Y, Li Q, Chen Q, Wu J, Luo E, et al. Critical summary and perspectives on state-of-health of lithium-ion battery. Renew Sustain Energy Rev. 2024;1;190:114077. https://doi.org/10.1016/J.RSER.2023.114077.

[25] Xiong W, Mo Y, Yan C. Online State-of-Health Estimation for Second-Use Lithium-Ion BatteriesBased on Weighted Least Squares Support Vector Machine. IEEE ACCESS. 2021;9:1870–81. https://doi.org/10.1109/ACCESS.2020.3026552.

[26] Zou B, Xiong M, Wang H, Ding W, Jiang P, Hua W, et al. A Deep Learning Approach for State-of-Health Estimation of Lithium-Ion-Batteries Based on a Multi-Feature and Attention Mechanism Collaboration. BATTERIES-BASEL. 2023; 9(6). https://doi.org/10.3390/batteries9060329.

[27] Zhou X, Hsieh SJ, Peng B, Hsieh D. Cycle life estimation of lithium-ion polymer batteries using artificialneural network and support vector machine with time-resolvedthermography. Microelectron Reliab. 2017;79:48–58. https://doi.org/10.1016/j.microrel.2017.10.013.

[28] Niraula A, Singh JG. Deep Learning-Based Approach for State-of-Health Estimation of Lithium-Ion Battery in the Electric Vehicles. 2023 Int Conf Power, Instrumentation, Energy Control PIECON 2023. https://doi.org/10.1109/PIECON56912.2023.10085757.

[29] Tang X, Zou C, Yao K, Chen G, Liu B, He Z, et al. A fast estimation algorithm for lithium-ion battery state of health. J Power Sources. 2018;31;396:453–8. https://doi.org/10.1016/J.JPOWSOUR.2018.06.036.

[30] Li Y, Dong B, Zerrin | Taner, Jauregui E, Wang X, Hua X, et al. State-of-health prediction for lithium-ion batteries via electrochemical impedance spectroscopy and artificial neural networks. Energy Storage. 2020; 1;2(5):e186. https://doi.org/10.1002/EST2.186.

[31] Huang S, Liu C, Sun H, Liao Q. State of health estimation of lithium-ion batteries based on theregional frequency. J Power Sources. 2022;518. https://doi.org/10.1016/j.jpowsour.2021.230773.

[32] Müller V, Scurtu RG, Memm M, Danzer MA, Wohlfahrt-Mehrens M. Study of the influence of mechanical pressure on the performance and aging of Lithium-ion battery cells. J Power Sources. 2019;15;440:227148. https://doi.org/10.1016/J.JPOWSOUR.2019.227148.

[33] Soltani M, Vilsen SB, Stroe AI, Knap V, Stroe DI. Degradation behaviour analysis and end-of-life prediction of lithium titanate oxide batteries. J Energy Storage. 2023;68. https://doi.org/10.1016/j.est.2023.107745.

[34] Chaoui H, Ibe-Ekeocha CC. State of Charge and State of Health Estimation for Lithium BatteriesUsing Recurrent Neural Networks. IEEE Trans Veh Technol. 2017; 66(10):8773–83. https://doi.org/10.1109/TVT.2017.2715333.

[35] Wang L, Pan C, Liu L, Cheng Y, Zhao X. On-board state of health estimation of LiFePO4 battery pack through differential voltage analysis. Appl Energy. 2016; 168:465–72. https://doi.org/10.1016/J.APENERGY.2016.01.125.

[36] Nemeth T, Schröer P, Kuipers M, Sauer DU. Lithium titanate oxide battery cells for high-power automotive applications – Electro-

thermal properties, aging behavior and cost considerations. J Energy Storage. 2020;31:101656. https://doi.org/10.1016/j.est.2020.101656.

[37] Lotfi N, Li J, Landers RG, Park J. Li-ion Battery State of Health Estimation based on an improved Single Particle model. Proc Am Control Conf. 2017 29;86–91. https://doi.org/10.23919/ACC.2017.7962935.

[38] Tan CM, Singh P, Chen C. Accurate Real Time On-Line Estimation of State-of-Health and RemainingUseful Life of Li ion Batteries. Appl Sci. 2020; 10(21). https://doi.org/10.3390/app10217836.

[39] Bloom I, Christophersen J, Gering K. Differential voltage analyses of high-power lithium-ion cells 2. Applications. J Power Sources. 2005;139(1–2):304–13. https://doi.org/10.1016/J.JPOWSOUR.2004.07.022.

[40] Bloom I, Christophersen JP, Abraham DP, Gering KL. Differential voltage analyses of high-power lithium-ion cells. 3. Another anode phenomenon. J Power Sources. 2006;157(1):537–42. https://doi.org/10.1016/J.JPOWSOUR.2005.07.054.

[41] Bloom I, Walker LK, Basco JK, Abraham DP, Christophersen JP, Ho CD. Differential voltage analyses of high-power lithium-ion cells. 4. Cells containing NMC. J Power Sources. 2010;195(3):877–82. https://doi.org/10.1016/J.JPOWSOUR.2009.08.019.

[42] Bloom I, Jansen AN, Abraham DP, Knuth J, Jones SA, Battaglia VS, et al. Differential voltage analyses of high-power, lithium-ion cells: 1. Technique and application. J Power Sources. 2005;139(1–2):295–303. https://doi.org/10.1016/J.JPOWSOUR.2004.07.021.

[43] McCulloch WS, Pitts W. A logical calculus of the ideas immanent in nervous activity. Bull Math Biophys. 1943;5(4):115–33. https://doi.org/10.1007/BF02478259.

[44] Dikmen IC, Karadag T. Electrical Method for Battery Chemical Composition Determination. IEEE Access. 2022;10:6496–504. https://doi.org/10.1109/ACCESS.2022.3143040.

[45] Zhang S, Zhai B, Guo X, Wang K, Peng N, Zhang X. Synchronous estimation of state of health and remaining useful lifetime for lithium-ion battery using the incremental capacity and artificial neural networks. J Energy Storage. 2019;26. https://doi.org/10.1016/J.EST.2019.100951.

[46] Cortes C, Vapnik V, Saitta L. Support-vector networks. Mach Learn. 1995;20(3):273–97. https://doi.org/10.1007/BF00994018.

[47] Cristianini N, Ricci E. Support Vector Machines. Encycl Algorithms. 2008;928–32. https://doi.org/10.1007/978-0-387-30162-4_415.

[48] Burges CJC. A Tutorial on Support Vector Machines for Pattern Recognition. Data Min Knowl Discov. 1998;2(2):121–67. https://doi.org/10.1023/A:1009715923555.

[49] Klass V, Behm M, Lindbergh G. A support vector machine-based state-of-health estimation method for lithium-ion batteries under electric vehicle operation. J Power Sources. 2014;270:262–72. https://doi.org/10.1016/J.JPOWSOUR.2014.07.116.

[50] Woldemariam W. A framework for transportation infrastructure cost prediction: a support vector regression approach. Transp Lett. 2022; https://doi.org/10.1080/19427867.2021.1985895.

[51] Li Q, Li D, Zhao K, Wang L, Wang K. State of health estimation of lithium-ion battery based on improved ant lion optimization and support vector regression. J Energy Storage. 2022;50:104215. https://doi.org/10.1016/J.EST.2022.104215.

[52] Zhang Y, Liu Y, Wang J, Zhang T. State-of-health estimation for lithium-ion batteries by combining model-based incremental capacity analysis with support vector regression. Energy. 2022;239:121986. https://doi.org/10.1016/J.ENERGY.2021.121986.

[53] M. PA, Wiener N. The Extrapolation, Interpolation and Smoothing of Stationary Time Series, with Engineering Applications. J R Stat Soc Ser A. 1950;113(3):413. https://doi.org/10.2307/2981007.

[54] Yu J. Online quality prediction of nonlinear and non-Gaussian chemical processes with shifting dynamics using finite mixture model based Gaussian process regression approach. Chem Eng Sci. 2012;82:22–30. https://doi.org/10.1016/J.CES.2012.07.018.

[55] Chen T, Ren J. Bagging for Gaussian process regression. Neurocomputing. 2009;72(7–9):1605–10. https://doi.org/10.1016/J.NEUCOM.2008.09.002.

[56] Bradford E, Imsland L. Stochastic Nonlinear Model Predictive Control Using Gaussian Processes. 2018 Eur Control Conf ECC 2018. 2018;1027–34. https://doi.org/10.23919/ECC.2018.8550249.

[57] Li F, Min Y, Zhang Y, Zhang Y, Zuo H, Bai F. State-of-health estimation method for fast-charging lithium-ionbatteries based on stacking ensemble sparse Gaussian process regression. Reliab Eng Syst Saf. 2024;242. https://doi.org/10.1016/j.ress.2023.109787.

[58] Su X, Sun B, Wang J, Zhang W, Ma S, He X, et al. Fast capacity estimation for lithium-ion battery based on online identification of low-frequency electrochemical impedance spectroscopy and Gaussian process regression. Appl Energy. 2022;322. https://doi.org/10.1016/j.apenergy.2022.119516.

[59] Zhou Y, Dong G, Tan Q, Han X, Chen C, Wei J. State of health estimation for lithium-ion batteries using geometric impedance spectrum features and recurrent Gaussian process regression. Energy. 2023; 262:125514. https://doi.org/10.1016/j.energy.2022.125514.

[60] Yang B, Qian Y, Li Q, Chen Q, Wu J, Luo E, et al. Critical summary and perspectives on state-of-health of lithium-ion battery. Renew Sustain Energy Rev. 2024;190:114077. https://doi.org/10.1016/j.rser.2023.114077.

[61] Dikmen IC, Yildiran N, Karadag T. Multi-Chemistry Battery Management System for Electric Vehicles. Eur J Res Dev. 2022;2(4):126–34. https://doi.org/10.56038/ejrnd.v2i4.176.

[62] Dikmen İC, Karadağ T. Onboard Battery Type Determination. In: 2021 5th International Symposium on Multidisciplinary Studies and Innovative Technologies (ISMSIT). 2021. p. 360–5. https://doi.org/10.1109/ISMSIT52890.2021.9604658.

[63] Karadağ T, Dikmen İC. Yeni Nesil, Modüler ve Akıllı Batarya Yönetim Sistemi. Avrupa Bilim ve Teknol Derg. 2021;(32):1103–12. https://doi.org/10.31590/ejosat.1045564.